

THREADED-FIELD-LINES MODEL FOR THE LOW SOLAR CORONA POWERED BY THE ALFVEN WAVE TURBULENCE

IGOR V. SOKOLOV¹, BART VAN DER HOLST¹, WARD B. MANCHESTER¹, DOGA CAN SU
OZTURK¹, JUDIT SZENTE¹, ALEKSANDRE TAKTAKISHVILI², GABOR TÓTH¹, MENG JIN^{3,4}, AND
TAMAS I. GOMBOSI¹

¹Climate and Space Sciences and Engineering, University of Michigan, 2455 Hayward St, Ann Arbor, MI
48109, USA

²Community Coordinated Modeling Center, NASA Goddard Space Flight Center, Greenbelt, MD 20771, USA

³Lockheed Martin Solar and Astrophysics Lab, Palo Alto, CA 94304, USA

⁴NASA/UCAR LWS Jack Eddy Fellow

ABSTRACT

We present an updated global model of the solar corona, including the transition region. We simulate the realistic three-dimensional (3D) magnetic field using the data from the photospheric magnetic field measurements and assume the magnetohydrodynamic (MHD) Alfvén wave turbulence and its non-linear dissipation to be the only source for heating the coronal plasma and driving the solar wind. In closed field regions the dissipation efficiency in a balanced turbulence is enhanced. In the coronal holes we account for a reflection of the outward propagating waves, which is accompanied by generation of weaker

counter-propagating waves. The non-linear cascade rate degrades in strongly imbalanced turbulence, thus resulting in colder coronal holes.

The distinctive feature of the presented model is the description of the low corona as almost-steady-state low-beta plasma motion and heat flux transfer along the magnetic field lines. We trace the magnetic field lines through each grid point of the lower boundary of the global corona model, chosen at some heliocentric distance, $R = R_b \sim (1.03 \div 1.15)R_\odot$ well above the transition region. One can readily solve the plasma parameters along the magnetic field line from 1D equations for the plasma motion and heat transport together with the Alfvén wave propagation, which adequately describe physics within the heliocentric distances range, $R_\odot < R < R_b$, in the low solar corona. By interfacing this threaded-field-lines model with the full MHD global corona model at $r = R_b$, we find the global solution and achieve a faster-than-real-time performance of the model.

Keywords: Sun: corona — Sun: transition region — Sun: EUV radiation

1. INTRODUCTION

Results from Hinode observations had upped the estimates for the magnetohydrodynamic (MHD) wave energetics in the solar corona ([De Pontieu et al. \(2007\)](#)). Observed in the chromosphere, the magnetic field perturbations carry a large enough energy to heat the solar corona and accelerate the solar wind. With the launch of the Solar Dynamics Observatory (SDO), we are now beginning to see observational hints of these ubiquitous waves in the transition region and low corona ([McIntosh et al. \(2011\)](#)).

Even before these encouraging observations had been obtained, models which incorporated, or were entirely based upon Alfvén wave turbulence as the momentum and energy source, were developed to describe the solar wind and coronal heating. In [Usmanov et al. \(2000\)](#), a three-dimensional (3D) model for the solar wind was suggested in which the Alfvén wave turbulence pressure served to accelerate the solar wind. The solar wind bi-modal structure as observed by Ulysses was successfully reproduced in the numerical simulation. However, the quantitative agreement of this model with the solar wind observations at 1 AU is insufficient for space weather simulations. The same criticism seems to be applicable to the more refined and physics-based Alfvén-wave-driven models of the solar wind by [Suzuki and Inutsuka \(2005\)](#); [Verdini et al. \(2010\)](#); [Osman et al. \(2011\)](#).

Therefore, the semi-empirical description of the solar wind so far has been used for space weather simulations, such as that adopted by [Arge and Pizzo \(2000\)](#) in their Wang-Sheeley-Arge (WSA) model. In [Cohen et al. \(2007\)](#), we coupled the semi-empirical WSA formulae for the solar wind speed at 1 AU to the global three-dimensional model for the solar corona and inner heliosphere. The WSA formulae were used as the boundary condition for the model which had been coupled to the MHD simulator via the varied polytropic index distribution (see [Roussev et al. \(2003\)](#)). However, the physics of the Alfvén wave turbulence has almost no intersection with the semi-empirical model of WSA.

Proceeding from the solar wind to the coronal heating, we can see again the disconnection between the physics-based models for the turbulent heating in the corona, one of the most advanced models of this kind being recently described in [Cranmer \(2010\)](#) (see also [Tu and Marsch \(1997\)](#); [Hu et al. \(2000\)](#); [Li and Habbal \(2003\)](#); [Dmitruk et al. \(2002\)](#)) on one hand, and well established models with semi-empirical heating function, such as that presented in

[Lionello et al. \(2001\)](#); [Riley et al. \(2006\)](#); [Titov et al. \(2008\)](#); [Lionello et al. \(2009\)](#); [Downs et al. \(2010\)](#), on the other hand. The heating function is applied to power the plasma in the solar corona with some heating rate, the distribution of which is given by some functions chosen not from some deep physical considerations, but rather in an ad-hoc manner to provide a better agreement with observations. In [Downs et al. \(2010\)](#) such thermodynamic MHD model had been used to explore empirical parameterizations of coronal heating in the context of realistic 3D magnetic structures observed in the EUV and soft-X-Rays. The observation synthesis capability has been extended to the major low corona imaging instruments available in space, namely STEREO/EUVI, SDO/AIA, and Hinode/XRT.

To overcome a disconnection between physics-based and observations-driven models, in [Sokolov et al. \(2013\)](#), we eliminated the *ad hoc* heating functions and parameterized the coronal heating in the Lower Corona (LC) in terms of the Alfvén wave turbulence dissipation. The boundary condition for the wave energy flux (the Poynting flux) inflowing to the solar corona from the solar surface appeared to be strongly restricted with observations, which reduces the model uncertainty. The difference in the plasma heating mechanism between open and closed field regions should be caused by a difference in the efficiency of wave dissipation due to nonlinear interaction between *oppositely propagating waves*. The degraded intensity of the inward propagating waves is responsible for the reduction in the turbulence dissipation rate in the coronal holes thus resulting in the bimodal solar wind structure. This Alfvén-Wave-driven SOLar Model (AWSOM) has been validated against observations by [Sokolov et al. \(2013\)](#); [Oran et al. \(2013\)](#); [van der Holst et al. \(2014\)](#).

The described global models simulate the steady state of the solar terrestrial environments, which serves as a background for *space weather*. Space weather describes the dynamic state

of the Earth’s magnetosphere-ionosphere system, which is driven by the solar wind and solar ionizing radiation. The greatest disturbances in space weather are geomagnetic storms, the most severe of which are caused by coronal mass ejections (CMEs) (see [Gosling \(1993\)](#)). While there are many magnetic driven models of CME initiation, these simulations are often performed in the domain of a Cartesian box (e.g. [Torok and Kliem \(2005\)](#)), or global models without the solar wind (e.g. [Antiochos et al. \(1999\)](#); [Fan and Gibson \(2004\)](#)). To date there have only been a few magnetically driven 3D MHD Sun-to-Earth CME models such as those by [Lugaz et al. \(2007\)](#); [Tóth et al. \(2007\)](#). The MHD simulation of [Tóth et al. \(2007\)](#) was able to come within 1.8 hours of the observed arrival time and came close to matching the overall field strength of the event. Recent examples of CME simulations performed with the use of AWSOM model for the solar corona and solar wind model are described in [Manchester et al. \(2012\)](#) and [Jin et al. \(2013\)](#).

Here we present the development of the AWSOM along two directions. First, we have been added recently (see [van der Holst et al. \(2014\)](#)) a quantitative model for reflection of the outward propagating waves, which is accompanied by generation of the counter-propagating waves in the coronal holes ultimately responsible for the turbulent cascade rate in these regions. The reflection models accounts for the gradients of the Alfvén speed as well as the plasma flow vorticity. The reflection due to strong magnetic field gradients may be also important in the close proximity of the active regions, intensifying the dissipation and the observable EUV emission.

The second distinctive feature of the presented model is the description of the low corona as almost-steady-state low-beta plasma motion along the magnetic field lines, the heat fluxes also being aligned with the magnetic field. The Low Solar Corona model which ranges from

upper chromosphere till the heliocentric distances about $(1.03 \div 1.15)R_{\odot}$ and includes the transition region, is the heart of the global models. In the Low Solar Corona the Alfvén waves pass from the chromosphere to the solar corona, the plasma temperature increases by two orders of magnitude (from ten thousand till million K), and this is also a place where the solar wind originates. The multi-wavelength observations (in EUV and X-rays) from several satellite locations (SDO, STEREO A,B) may be used to validate the simulation model. Therefore, any global model must account for the processes in this region. On the other hand, for the simulation model to explain the space weather and also have a predictive capability, it should be capable of simulating the dynamic processes faster than they proceed in real time, and the Low Solar Corona appears to be a bottleneck limiting the computational efficiency and performance.

In numerical simulations of the solar corona, both for the ambient state and especially for dynamical processes, the greatest number of computational resources is spent for maintaining the numerical solution in the Low Solar Corona and in the transition region, where the temperature gradients are sharp and the magnetic field topology is complicated. The degraded computational efficiency is caused by the need for the highest resolution as well as the use of a fully three-dimensional implicit solver for electron heat conduction. The need to find a numerical method, which would allow us to gain in the computational efficiency, motivates the research presented here.

We benefit from the observation that although the simulations of the Low Solar Corona are computationally intense, the physical nature of the processes involved is rather simple as long as the heat fluxes and slow plasma motional velocities are mostly aligned with the magnetic field. The Alfvén wave turbulence, is characterized by the wave Poynting flux, which is

also aligned with the magnetic field. Therefore, the plasma state at any point within the Low Solar Corona is controlled by the plasma, particle, and Alfvén wave transport along the magnetic field line, which passes through this point. This physical property is typical for a variety of magnetized plasmas in different astrophysical and laboratory environments and may be used as the base of a new numerical method, which solves the state of plasma in each grid point in the computational domain depth in the following way: (1) by passing the magnetic field line ('thread') through this point and connecting it with the domain boundaries (e.g., with chromosphere and with the global solar corona domain, once the method is applied to the Low Solar Corona) and (2) by solving a set of one-dimensional transport equations to relate the grid point value to the boundary conditions.

We trace the magnetic field lines through all grid points of the lower boundary of the global coronal model chosen at some heliocentric distance $R = R_b \sim (1.03 \div 1.15)R_\odot$ well above the transition region. One can readily solve the plasma parameters along the magnetic field line from effectively 1D equations for the plasma motion and heat transfer together with the Alfvén wave propagation, which adequately describe physics within the heliocentric distance range, $R_\odot < R < R_b$, i.e. in the low solar corona. By interfacing this Threaded-Field-Line Model (TFLM) for the low corona with full MHD global corona model at $R = R_b$ we find the global solution and achieve faster-than-realtime efficiency of the model. Due to the latter feature we call the newly developed model AWSoM-R (AWSoM-Realtime).

2. MHD EQUATIONS FOR THE TRANSITION REGION, SOLAR CORONA AND INNER HELIOSPHERE

2.1. *Full 3D Governing Equations of the Global Model*

The global model within the range of heliocentric distances, $R_b < R < 1 \div 3$ AU ($R_b \sim (1.03 \div 1.15)R_\odot$) employs the standard MHD equations (non-specified denotations are as usually):

$$\frac{\partial \rho}{\partial t} + \nabla \cdot (\rho \mathbf{u}) = 0, \quad (1)$$

$$\frac{\partial \mathbf{B}}{\partial t} + \nabla \cdot (\mathbf{u} \mathbf{B} - \mathbf{B} \mathbf{u}) = 0, \quad (2)$$

$$\frac{\partial(\rho \mathbf{u})}{\partial t} + \nabla \cdot \left(\rho \mathbf{u} \mathbf{u} - \frac{\mathbf{B} \mathbf{B}}{\mu_0} \right) + \nabla \left(P_i + P_e + \frac{B^2}{2\mu_0} + P_A \right) = -\frac{GM_\odot \rho \mathbf{R}}{R^3}, \quad (3)$$

(herewith, $B = |\mathbf{B}|$), with the full energy equations applied separately to ions

$$\begin{aligned} & \frac{\partial}{\partial t} \left(\frac{P_i}{\gamma - 1} + \frac{\rho u^2}{2} + \frac{\mathbf{B}^2}{2\mu_0} \right) + \nabla \cdot \left\{ \left(\frac{\rho u^2}{2} + \frac{\gamma P_i}{\gamma - 1} + \frac{B^2}{\mu_0} \right) \mathbf{u} - \frac{\mathbf{B}(\mathbf{u} \cdot \mathbf{B})}{\mu_0} \right\} = \\ & = -(\mathbf{u} \cdot \nabla)(P_e + P_A) + \frac{N_e N_i k_B}{\gamma - 1} \left(\frac{\nu_{ei}}{N_i} \right) (T_e - T_i) + f_p (\Gamma_- w_- + \Gamma_+ w_+) - \frac{GM_\odot \rho \mathbf{R} \cdot \mathbf{u}}{R^3}, \end{aligned} \quad (4)$$

and to electrons:

$$\begin{aligned} & \frac{\partial \left(\frac{P_e}{\gamma - 1} \right)}{\partial t} + \nabla \cdot \left(\frac{P_e}{\gamma - 1} \mathbf{u} \right) + P_e \nabla \cdot \mathbf{u} = \\ & = \nabla \cdot (\kappa \cdot \nabla T_e) + \frac{N_e N_i k_B}{\gamma - 1} \left(\frac{\nu_{ei}}{N_i} \right) (T_i - T_e) - Q_{\text{rad}} + (1 - f_p) (\Gamma_- w_- + \Gamma_+ w_+), \end{aligned} \quad (5)$$

where, for a hydrogen plasma, $N_e = N_i = \rho/m_p$, m_p being the proton mass. In addition to the standard effects, the above equations account for the radiation energy loss from an optically thin plasma, $Q_{\text{rad}} = N_e N_i \Lambda(T_e)$, a possible difference in the electron and ion temperatures, $T_{e,i}$, the electron heat conduction parallel to the magnetic field lines equals:

$$\kappa = \mathbf{b} \mathbf{b} \kappa_{\parallel}, \quad \kappa_{\parallel} = 3.2 \frac{6\pi}{L_C} \sqrt{\frac{2\pi}{m_e}} \left(\frac{\varepsilon_0}{e^2} \right)^2 (k_B T_e)^{5/2} k_B, \quad \mathbf{b} = \mathbf{B}/B, \quad (6)$$

where m_e and e are the electron mass and charge correspondingly, L_C being the Coulomb logarithm. The energy exchange between electron and ions is parameterized via the energy exchange rate, $\frac{\nu_{ei}}{N_i} = \frac{2\sqrt{m_e} L_C (e^2/\varepsilon_0)^2}{3m_p (2\pi k_B T_e)^{3/2}}$, as this is usually done. The Alfvén wave turbulence pressure, $P_A = (w_- + w_+)/2$, and dissipation rate, $\Gamma_- w_- + \Gamma_+ w_+$, are applied in the above

equations. Herewith, w_{\pm} are the energy densities for the turbulent waves propagating along the magnetic field vector (w_+) or in the opposite direction (w_-). The turbulence energy dissipation (see Eqs.4-5) is split into electron and ion heating. For simplicity, we assume a constant fraction of energy, $f_p \approx 0.6$, dissipated into ions, the problems caused by this assumption are discussed below. At higher densities as in the low corona, we assume $T_e = T_i$ and use the single-temperature energy equation for electron and ions, to improve the computational efficiency:

$$\begin{aligned} \frac{\partial}{\partial t} \left(\frac{P}{\gamma - 1} + \frac{\rho u^2}{2} + \frac{\mathbf{B}^2}{2\mu_0} \right) + \nabla \cdot \left\{ \left(\frac{\rho u^2}{2} + \frac{\gamma P}{\gamma - 1} + \frac{B^2}{\mu_0} \right) \mathbf{u} - \frac{\mathbf{B}(\mathbf{u} \cdot \mathbf{B})}{\mu_0} \right\} = \\ = -(\mathbf{u} \cdot \nabla)P_A + \nabla \cdot (\kappa \cdot \nabla T) - Q_{\text{rad}} + \Gamma_- w_- + \Gamma_+ w_+ - \frac{GM_{\odot} \rho \mathbf{r} \cdot \mathbf{u}}{r^3}, \end{aligned} \quad (7)$$

where $P = P_e + P_i = 2N_i k_B T$. We use the equation of state, $P_{e,i} = N_{e,i} k_B T_{e,i}$ for the coronal plasma with the polytropic index, $\gamma = \frac{5}{3}$. To complete the model, the equation describing propagation, reflection and dissipation of turbulent waves has been derived in *van der Holst et al. (2014)* following the approach as adopted in *Velli (1993)*; *Chandran et al. (2009)*; *Chandran and Hollweg (2009)*; *Dmitruk et al. (2002)*; *Tu and Marsch (1995)*):

$$\frac{\partial w_{\pm}}{\partial t} + \nabla \cdot [(\mathbf{u} \pm \mathbf{V}_A)w_{\pm}] + \frac{w_{\pm}}{2}(\nabla \cdot \mathbf{u}) = \mp \mathcal{R} \sqrt{w_- w_+} - \Gamma_{\pm} w_{\pm} \quad (8)$$

where $\Gamma_{\pm} = \frac{2}{L_{\perp}} \sqrt{\frac{w_{\mp}}{\rho}}$ (note that the definition of L_{\perp} and, accordingly the expression for Γ_{\pm} used both here and in *van der Holst et al. (2014)* are by a factor of 2 different from those used in *Sokolov et al. (2013)*). The reflection coefficient has been found as follows:

$$\begin{aligned} \mathcal{R} = \min \left\{ \sqrt{(\mathbf{b} \cdot [\nabla \times \mathbf{u}])^2 + [(\mathbf{V}_A \cdot \nabla) \log V_A]^2}, \max(\Gamma_{\pm}) \right\} \times \\ \times \left[\max \left(1 - \frac{I_{\text{max}}}{\sqrt{w_+/w_-}}, 0 \right) - \max \left(1 - \frac{I_{\text{max}}}{\sqrt{w_-/w_+}}, 0 \right) \right], \end{aligned} \quad (9)$$

where $I_{\max} = 2$ is the maximum "imbalance degree". If the "plus" wave strongly dominates, so that $\sqrt{w_+/w_-} > I_{\max}$, the multiplier in the second line tends to +1, in the opposite limiting case of the dominant "minus" wave, it tends to -1. In both these cases the reflection reduces the dominant wave and amplifies the minor one. Otherwise, if the both amplitude ratios do not exceed I_{\max} , the turbulence is treated as "balanced" and the reflection coefficient turns to zero. The reflection model used in ([Matthaeus et al. 1999](#)) was ideologically similar to ours.

The important distinction is that we don't introduce the incompressible-to-compressible mode conversion term proportional to $(\mathbf{u} \cdot \nabla) \log V_A$ into our model, although it is sometimes accounted for by other authors. The reason for this omission is that this term would break the energy conservation in the model as long as it describes the conversion to the compressible MHD turbulence, which is not included (for more detail see [van der Holst et al. \(2014\)](#)).

The boundary condition for the Poynting flux is given by $\frac{\Pi_{R_\odot}}{B_{R_\odot}} = \text{const} = \left[\frac{\Pi}{B}\right]$. The estimate of the *constant* Pointing-flux-to-field ratio at the solar surface may be found in [Sokolov et al. \(2013\)](#); [Oran et al. \(2013\)](#); [van der Holst et al. \(2014\)](#): $\left[\frac{\Pi}{B}\right] \approx 1.1 \cdot 10^6 \frac{\text{W}}{\text{m}^2\text{T}}$, where the boundary condition for the wave energy density should be applied to the outgoing wave only. The estimate is very close to that which follows from [Pevtsov et al. \(2003\)](#); [Abbett \(2007\)](#); [Downs et al. \(2010\)](#); [Cranmer \(2010\)](#); [Suzuki \(2006\)](#). To close the model we chose, following [Hollweg \(1986\)](#), the scaling law for the transverse correlation length:

$$L_\perp \propto B^{-1/2}, \quad 100 \text{ km} \cdot \text{T}^{1/2} \leq [L_\perp \sqrt{B}] \leq 300 \text{ km} \cdot \text{T}^{1/2}. \quad (10)$$

2.1.1. *Alternative 3D equations for Alfvén Wave Dynamics*

Eq.(8) has a form close to the conservation law, which is well suited for solving it numerically within the framework of the global coronal model. However, both for using in the TFLM model and for analytical solution, an alternative form of this equation may be derived based on the substitution, $w_{\pm} = [\Pi/B]\sqrt{\mu_0\rho}a_{\pm}^2$. With an account of the mass conservation law, one obtains:

$$\frac{\partial a_{\pm}^2}{\partial t} + \nabla \cdot (\mathbf{u}a_{\pm}^2) \pm (\mathbf{V}_A \cdot \nabla)a_{\pm}^2 = \mp \mathcal{R}a_{-}a_{+} - 2\sqrt{\frac{[\Pi/B]\mu_0V_A}{[L_{\perp}\sqrt{B}]^2}}a_{\mp}a_{\pm}^2. \quad (11)$$

The plasma heating function, $\Gamma_+w_+ + \Gamma_-w_-$, in these denotations equals

$$\Gamma_+w_+ + \Gamma_-w_- = 2(a_+ + a_-)a_+a_-[\Pi/B]B\sqrt{\frac{[\Pi/B]\mu_0}{[L_{\perp}\sqrt{B}]^2V_A}}. \quad (12)$$

The dimensionless amplitude, a_{\pm} , of the outgoing wave at the lower boundary of the model equals unity. In Eqs.(11) the dimensionless wave amplitudes depend on the plasma dynamical profile only via the plasma velocity as well as the Alfvén speed. In the inner heliosphere, in neglecting the Alfvén speed and assuming steady state radial solar wind motion with the constant speed (i.e. independent on the heliocentric distance), the dimensional amplitude and the total turbulence energy density decay with the heliocentric distance as follows: $(a_+^2 + a_-^2) \propto 1/R^2$, $\rho \propto 1/R^2$, and $(w_+ + w_-) \propto 1/R^3 \propto \rho^{3/2}$, the latter relationship being in agreement with the polytropic index of 3/2, for the Alfvén wave turbulence. In the low Solar Corona the Alfvén wave turbulence dynamics is more complicated and discussed below.

2.2. Equations of the Threaded-Field-Line Model

Now, the governing AWSOM equations may be applied to simulate the transition region and Low Solar Corona domain at $R_{\odot} < R < R_b$. We present both the simplified 1D model equations for this domain and the way how the model may be interfaced both to the chromosphere at $R \rightarrow R_{\odot}$ and to the global corona model at $R \rightarrow R_{\odot}$.

2.2.1. Magnetic field

The realistic model for the 3d solar magnetic field includes the boundary condition for the coronal magnetic field taken from the full disc magnetogram incorporating the current and past observation results. The potential magnetic field provides the minimum of magnetic free energy, therefore, in the "ambient" solution for the solar wind the magnetic field is approximately equal to the potential one in the close proximity of the Sun. Following [Ogino and Walker, \(1984\)](#); [Tanaka \(1994\)](#) (see also [Powell et al. \(1999\)](#); [Gombosi et al., \(2002\)](#)) we split the total magnetic field $\mathbf{B} = \mathbf{B}_0 + \mathbf{B}_1$, in such way that the *potential* \mathbf{B}_0 field dominates at $R \rightarrow R_\odot$. If the observable is the radial component of the magnetic field at the photospheric level, then the potential \mathbf{B} field may be recovered from the observed magnetogram using the Potential Field Source Surface Method (PFSSM) had been for the first time described in [Altschuler et al \(1977\)](#). The Laplace equation for scalar magnetic potential is solved at $R_\odot < R < R_{SS} = 2.5R_\odot$ with the given radial gradient of the potential (the observed radial field) at $R = R_\odot$ and with vanishing magnetic potential (i.e. purely radial magnetic field) at $R = R_{SS}$, using the development into a series of spherical harmonics. Accordingly, non-potential \mathbf{B}_1 field within the original split field approach (used, particularly, in [Sokolov et al. \(2013\)](#); [Oran et al. \(2013\)](#); [van der Holst et al. \(2014\)](#)) satisfies zero boundary condition for the radial field component, $(\mathbf{B}_1)_R = 0$, at $R = R_\odot$, as long as the observed field is fully included into the potential field.

The distinction of the approach presented here is that we neglect non-potential \mathbf{B}_1 field in the Low Corona and assume that $\mathbf{B}_1 \equiv 0$ at $R_\odot < R < R_b$. Accordingly, the boundary condition, $(\mathbf{B}_1)_R = 0$, is accepted within the global model at $R = R_b$. In this way we benefit in easily bridging the field observed at $R = R_\odot$ to the model starting at $R = R_b$. Second, the

lines of the potential, \mathbf{B}_0 , field at $R_\odot < R < R_b$ give us the *threads* which allow us to bridge the boundary conditions for all other physical quantities from the top of chromosphere to the global model boundary at $R = R_b$.

2.2.2. Magnetic thread and the conservation laws on it.

Now, we introduce a key concept of the Threaded-Field-Line Model (TFLM) - a thread. The boundary conditions for the global model are to be applied at each grid point of the global model boundary at $R = R_b$. The *potential* magnetic field line, "thread", starting at the grid point can be traced through the Low Corona domain, $R_\odot < R < R_b$ toward the Sun. To reduce the 3D governing equations to effectively 1D equations, one can integrate Eqs.(1,3,7) over a magnetic flux tube element of a length of ds bounded by two close cross sections of the flux tube, dS_1 and dS_2 , and a bundle of magnetic field lines about the considered thread, which all pass through the contours of these cross sections. The equation, $\nabla \cdot \mathbf{B} = 0$ gives: $BdS = \text{const}$ along the flux tube, which allows us to relate the change in the cross-section area along the thread to the magnetic field magnitude. The conservation laws are greatly simplified due to the fact that the velocity of low-beta plasma motion is aligned with the magnetic field. Particularly, the continuity equation (1) for a steady-state flow along the flux tube gives: $\frac{\partial}{\partial s} \left(\frac{\rho u}{B} \right) = 0$ and

$$\left[\frac{\rho u}{B} \right] = \text{const}, \quad (13)$$

where $u = (\mathbf{b} \cdot \mathbf{u})$ is the velocity aligned with the magnetic field and $\frac{\partial}{\partial s} = (\mathbf{b} \cdot \nabla)$. Herewith we denote with square brackets the combinations of variables, which are constant along the thread (above we did this only for the model parameters, $[\Pi/B]$ and $[L_\perp \sqrt{B}]$).

In the momentum equation we neglect u^2 comparing with the speed of sound squared,

$\gamma P/\rho$ and omit $\mathbf{j} \times \mathbf{B}$ force, vanishing in the potential magnetic field ($\mathbf{j} \propto \text{curl} \mathbf{B}_0 = 0$), which gives us the hydrostatic equilibrium equation:

$$\frac{\partial P}{\partial s} = -\frac{b_R G M_\odot \rho}{R^2}. \quad (14)$$

The latter can be integrated, if desired, for the given profile of temperature giving the barometric formula, $P = P_{TR} \exp \left[\int_{R_{TR}}^R \frac{d(G M_\odot m_p / R)}{2 k_B T} \right]$, the values of variables on top of the transition region (TR) are discussed below. As long as the velocity is not solved within the TFLM, the parameter as in Eq.(13) should be found from the Global Corona Model (GCM) side: $\left(\frac{u}{B}\right)_{TFLM} = \lim_{R \rightarrow R_b+0} ((\mathbf{B} \cdot \mathbf{u})/B^2)_{GCM}$.

In Eq.(7) we keep the time derivative of temperature as long as the electron heat conduction is a comparatively slow process:

$$\begin{aligned} & \frac{2N_i k_B}{B(\gamma-1)} \frac{\partial T}{\partial t} + \frac{2k_B \gamma}{(\gamma-1)} \left[\frac{N_i u}{B} \right] \frac{\partial T}{\partial s} = \\ & = \frac{\partial}{\partial s} \left(\frac{\kappa_{\parallel}}{B} \frac{\partial T}{\partial s} \right) + \frac{\Gamma_- w_- + \Gamma_+ w_+ - N_e N_i \Lambda(T)}{B} + \left[\frac{\rho u}{B} \right] \frac{\partial(G M_\odot / r)}{\partial s}. \end{aligned} \quad (15)$$

Note, that we neglect the Alfvén wave pressure gradients in Eqs.(14,15). Practically in the Low Corona this pressure is small, being proportional to a square root of high density, while the thermal pressure is proportional to the density. Theoretically, an account for this term in Eq.(15) would be inconsistent. Comparing with the Alfvén wave energy deposition (see below) it involves the small ratio of the plasma speed to the Alfvén wave speed, and all such terms are neglected in deriving Eq.(16) below.

2.2.3. Alfvén wave 1D dynamics.

The physical property of the Alfvén Waves to have the energy flux aligned with the magnetic field allows us to reduce 3D differential operators in the governing equations to the advective derivatives along the magnetic field lines. In addition, the 1D governing equations,

which are obtained in this way, may be further simplified for the low corona environments. Indeed, in the low solar corona the plasma velocity in Eqs.(11) is negligible as comparing with the Alfvén wave speed. The steady-state solutions for a_{\pm} may be sought for, as long as the non-stationary perturbations propagate with the large Alfvén wave speed across the low corona and fast converge to an equilibrium, so that Eqs(11) once divided by V_A may be written as follows: $\pm(\mathbf{b} \cdot \nabla)a_{\pm}^2 = \mp \frac{\mathcal{R}}{V_A}a_-a_+ - 2\sqrt{\frac{[\Pi/B]\mu_0}{[L_{\perp}\sqrt{B}]^2V_A}}a_{\mp}a_{\pm}^2$ This equation may be further simplified by substituting $d\xi = ds\sqrt{\frac{[\Pi/B]\mu_0}{[L_{\perp}\sqrt{B}]^2V_A}}$:

$$\pm \frac{da_{\pm}}{d\xi} = \mp \frac{ds}{d\xi} \frac{\mathcal{R}}{2V_A}a_{\mp} - a_-a_+. \quad (16)$$

As long as the plasma speed is small comparing with the Alfvén speed, the velocity curl in the expression for the reflection coefficient is negligible comparing with the contribution from the Alfvén speed gradient, hence:

$$\frac{ds}{d\xi} \frac{\mathcal{R}}{2V_A} = \min \left(\frac{|d \log V_A / d\xi|}{2a_{\max}}, 1 \right) (\max(a_{\max} - 2a_-, 0) - \max(a_{\max} - 2a_+, 0)), \quad (17)$$

$a_{\max} = \max(a_-, a_+)$. The formulation of the boundary-value-problem assumes that at the starting point of the magnetic field line, i.e. at minimal $\xi = \xi_-$, the boundary value a_{+0} should be given for a_+ wave, propagating in the direction of increasing ξ : $a_+(\xi = \xi_-) = a_{+0}$. For the oppositely propagating wave the boundary value, a_{-0} , should be given at the right end point $\xi = \xi_+$, of the magnetic field line section, $[\xi_-, \xi_+]$: $a_-(\xi = \xi_+) = a_{-0}$. For the case of the closed magnetic field line, starting and ending at the solar surface, $a_{+0} = a_{-0} = 1$ because of our choice of the Boundary Condition (BC) for the Poynting flux. A few examples of the problem formulation for Eq.(16) are delegated to Section 3.

In Eq.(15) one can express $(\Gamma_-w_- + \Gamma_+w_+)/B = 2(a_- + a_+)a_-a_+d\xi/ds[\Pi/B] = d(a_-^2 -$

$a_+^2)/ds[\Pi/B]$ and on dividing Eq.(15) by $[\Pi/B]$, it can be rewritten as follows:

$$\begin{aligned} & \frac{2N_i k_B}{[\Pi/B]B(\gamma-1)} \frac{\partial T}{\partial t} + \frac{\partial}{\partial s} \left\{ \left[\frac{N_i u}{[\Pi/B]B} \right] \frac{2k_B \gamma T}{(\gamma-1)} - \frac{\kappa_0 T^{5/2}}{[\Pi/B]B} \frac{\partial T}{\partial s} \right\} = \\ & = -\frac{N_e N_i \Lambda(T)}{[\Pi/B]B} + \frac{\partial}{\partial s} \left\{ a_-^2 - a_+^2 + \left[\frac{N_i u}{[\Pi/B]B} \right] \frac{GM_\odot m_p}{R} \right\} \end{aligned} \quad (18)$$

In application to the TFLM it is convenient to denote with "+" and "-" subscripts the waves propagating outward and inward correspondingly and assume that the variable s along the thread equals zero at the solar surface and is positive at $R_\odot < R < R_b$. These assumptions require to re-define the BCs at the interface $R = R_b$ between the TFLM and GC models as follows:

$$\begin{aligned} b_R|_{R=R_b} > 0 : \left(\frac{u}{B} \right)_{TFLM} &= \left(\frac{(\mathbf{B} \cdot \mathbf{u})}{B^2} \right)_{GCM}, (a_-)_{TFLM} = (a_-)_{GCM}, (a_+)_{GCM} = (a_+)_{TFLM} \\ b_R|_{R=R_b} < 0 : \left(\frac{u}{B} \right)_{TFLM} &= - \left(\frac{(\mathbf{B} \cdot \mathbf{u})}{B^2} \right)_{GCM}, (a_-)_{TFLM} = (a_+)_{GCM}, (a_-)_{GCM} = (a_+)_{TFLM} \end{aligned}$$

2.2.4. BCs for temperature and density

The temperature is governed by Eq.(18) which is of the second order with respect to the spatial coordinate. Hence, at the interface between TFLM and GCM both temperature and its gradient should be continuous, so that the BC for temperature within the TFLM may be taken from the GCM: $T_{TFLM} = T_{GCM}$ at $R = R_b$. Accordingly, once the TFLM equations have been solved with the given temperature at $R = R_b$ and the BC at $R = R_\odot$ as discussed below, the gradient, $(\frac{\partial T}{\partial s})_{TFLM}$, at $R = R_b$ is known and can be used to set the radial temperature gradient within the GCM. Assuming the radial component of the temperature gradient to be dominant, one has: $(\frac{\partial T}{\partial s})_{GCM} \approx (\frac{\partial T}{\partial R})_{GCM}$. Hence, the equation, $(\frac{\partial T}{\partial R})_{GCM} = (\frac{\partial T}{\partial s})_{TFLM} / |b_R|$, may be used to close the boundary value problem in the GCM by setting the heating flux through the interface between TFLM and GCM.

The density at the discussed interface is controlled by the direction of u . If $u > 0$, then $[\frac{N_i u}{B}]_{TFLM} = (N_i)_{TFLM} (\frac{u}{B})_{GCM}$, otherwise $[\frac{N_i u}{B}]_{TFLM} = (\frac{N_i u}{B})_{GCM}$. All we need now in order to get well-posed problem for the listed 1D governing equations is to close the model with the boundary condition at "low boundary". A good opportunity is to set the boundary conditions *on top of the Transition Region* (TR), which may be matched with the chromosphere via an *analytical model* of the transition region. This model had been presented in [Lionello et al. \(2001\)](#) (see also [Lionello et al. \(2009\)](#); [Downs et al. \(2010\)](#)).

To use this model, we choose at each magnetic thread a short section of the length of, $L_{TR} = \int_{R_\odot}^{R_{TR}} ds \sim 1$ Mm to be a width of the TR along the magnetic field line. This is an important distinction from previous works, in which the temperature on top of the TR had been set, rather than the TR width. In the steady-state version of Eq.(18) we keep only the terms which dominate within the TR, i.e. at high density and abrupt temperature gradients:

$$-\frac{\partial}{\partial s} \left(\kappa_0 T^{5/2} \frac{\partial T}{\partial s} \right) = -N_e N_i \Lambda(T). \quad (19)$$

On multiplying Eq.(19) by $\kappa_0 T^{5/2} (\partial T / \partial s)$ and by integrating from the interface to chromosphere till a given point at a temperature, T , one can obtain:

$$\frac{1}{2} \kappa_0^2 T^5 \left(\frac{\partial T}{\partial s} \right)^2 \Big|_{T_{ch}}^T = [N_i T]^2 \int_{T_{ch}}^T \kappa_0 T_1^{1/2} \Lambda(T_1) dT_1. \quad (20)$$

Here the product, $[N_i T]$ is assumed to be constant, therefore, it is separated from the integrand, as long as the temperature gradient scale within the TR is much shorter than the barometric scale: $T / (\partial T / \partial s) \ll k_B T / (G M_\odot m_p / R_\odot^2)$. On the left hand side of the equation the half of the heat flux squared should be taken at the temperature, T , with the positive sign and at temperature T_{ch} with negative sign. We can neglect the contribution from the latter term at the lower boundary of this transition region, if we postulate that the tran-

sition region is heated solely by the heat transfer from the corona and the lower boundary of the transition region is where the heat flux from the corona turns to zero. For given $T_{ch} \sim (1 \div 2) \cdot 10^4$ K and L_{TR} one can solve $[N_i T]$ in terms of the radiation loss integral:

$$[N_i k_B T] = \frac{1}{L_{TR}} \int_{T_{ch}}^{T_{TR}} \frac{\kappa_0 T_1^{5/2} dT_1}{U_{\text{heat}}(T_1)}, \quad U_{\text{heat}}(T) = \sqrt{\frac{2}{k_B^2} \int_{T_{ch}}^T \kappa_0 (T')^{1/2} \Lambda(T') dT'}, \quad (21)$$

which also allows us to find the heat flux into the TR from the Low Corona:

$$\kappa_0 T_{TR}^{5/2} \left(\frac{\partial T}{\partial s} \right)_{T=T_{TR}} = [N_i k_B T] U_{\text{heat}}(T_{TR}). \quad (22)$$

Here, U_{heat} is a quantity with the dimension of speed, such that $2L_{TR}/((\gamma - 1)U_{\text{heat}}(T_{TR}))$ is a typical temperature relaxation time in the TR.

We arrive at nonlinear boundary conditions on top of the TR, which for the known width L_{TR} , of the TR and for a given temperature, T_{TR} , on top of the TR allow us to find the heat flux and pressure there using Eqs.(21,22). These BC may be easily implemented if the temperature functions in the right hand side of Eqs.(21,22) as well as the function, $\Lambda(T)$, are all tabulated using CHIANTI database (see Fig.1). Now, the TFLM is fully described and designed to be solved numerically. There is still a minor uncertainty in the way to distinguish the TR from the top of chromosphere, originating from the fact, that we do not include a consistent chromosphere model. Particularly, the TR solution at some point should be merged to the chromosphere solution with no jump in pressure, at the location, which depends both on $[N_i k_B T]_{TR}$ and on the pressure barometric distribution in the chromosphere. However, the uncertainty in this location, which also results in some uncertainty in L_{TR} , is negligible as long as the barometric scale in the chromosphere is small.

3. ANALYTICAL SOLUTIONS AND SCALING LAWS FOR THE ALFVÉN WAVE TURBULENCE IN THE LOW SOLAR CORONA

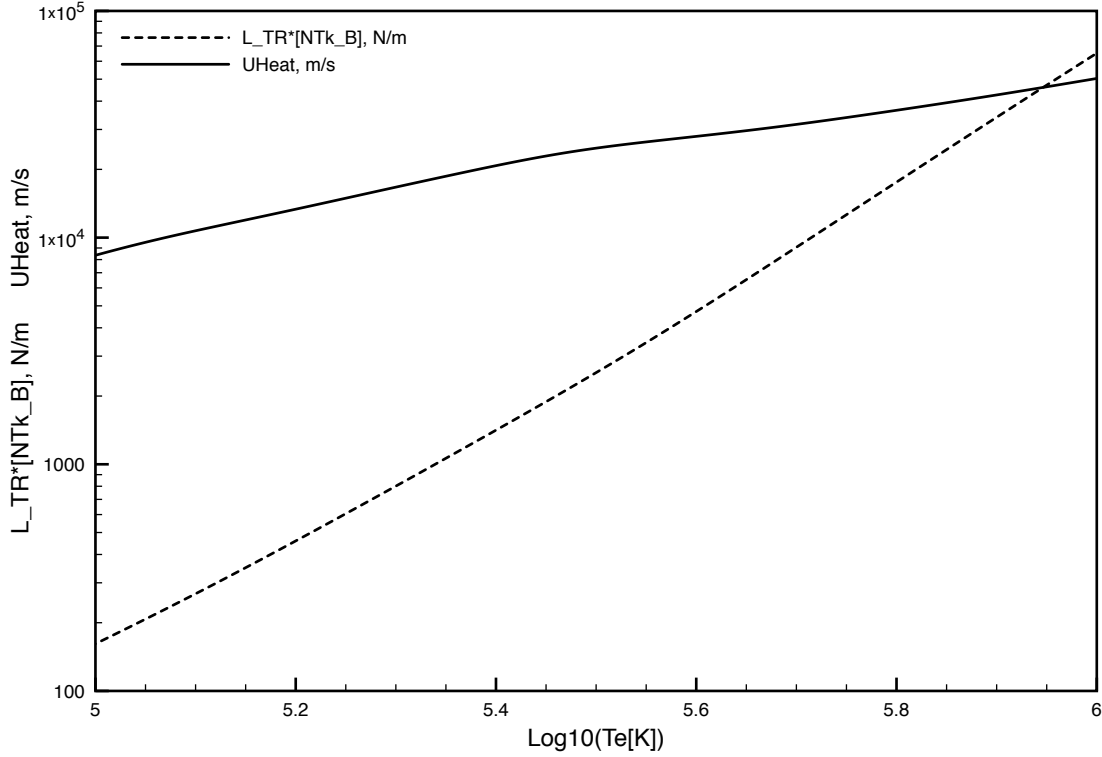


Figure 1. Preprocessed CHIANTI table for radiative cooling, which allows us to formulate the boundary condition at the solar surface, for the TFLM. For a known width, L_{TR} , of the internal transition region and for the input temperature, T , the constant product, $[NTk_B]$ may be found using the dashed curve. Then, the heat flux into the transition region, $U_{\text{heat}}[NTk_B]$, may be found using also the solid curve.

As has been demonstrated above, the main point of the developed approach is to achieve efficient and realistic modeling of the solar atmosphere. On the other hand, the analytical solutions, discussed in the present Section are over-simplified and are relevant only for analyzing the equations describing to the Alfvén wave dynamics. Although these solutions are not directly usable for doing simulations, they may give hints on dependencies between the different model parameters. Of a particular interest is the question, which model parameters should be modified to achieve a better agreement with the observations of the solar wind parameters at 1 AU. Therefore, we provide here some solutions describing the wave turbulence

in the different regions (closed vs open field lines, lower vs global SC etc).

3.1. *Solution for Coronal Holes - Weak Reflection*

Here, we consider an open magnetic field line, by assuming as we did above, that the wave of amplitude, a_+ , propagates outward the Sun. First, consider the case when the reflection due to a gradual change in the Alfvén speed magnitude (the latter is assumed to exponentially decay outward the Sun, $V_A = V_{A0} \exp(-s/L_{V_A})$) is small comparing with the characteristic dissipation rate: $\frac{1}{2} \frac{ds}{d\xi} \frac{|\mathcal{R}|}{V_A} = \frac{1}{2} \frac{d \log V_A}{d\xi} \ll a_+$. This assumption is valid at sufficiently high altitudes much above the transition region (in which, to the contrary the abrupt density gradients cause large reflection as we discuss below). As the result of a weak reflection, the amplitude of the wave reflected back and propagating toward the Sun is small: $a_- \ll a_+$. The governing equations in this limiting case read:

$$\frac{da_+}{d\xi} = \frac{1}{2} \frac{d \log V_A}{d\xi} a_- - a_- a_+, \quad \frac{da_-}{d\xi} = \frac{1}{2} \frac{d \log V_A}{d\xi} a_+ + a_- a_+ \quad (23)$$

For the exponentially decaying profile of the Alfvén speed, by introducing a constant small parameter:

$$C_{\text{refl}} = -\frac{1}{2} \frac{d \log V_A}{d\xi} \sqrt{\frac{V_{A0}}{V_A}} = \frac{1}{2} \sqrt{\frac{[L_\perp \sqrt{B}]^2 V_{A0}}{L_{V_A}^2 [\Pi/B] \mu_0}} = 0.09 \frac{[L_\perp \sqrt{B}]}{150 \text{ km T}^{1/2}} \frac{R_\odot}{L_{V_A}} \sqrt{\frac{V_{A0}}{10^3 \text{ km/s}} \frac{1.1 \cdot 10^6 \frac{\text{W}}{\text{m}^2 \text{T}}}{[\Pi/B]}},$$

one can easily find the solution of Eqs.(eq:weakrefl), tending to zero at infinity:

$$a_+ = \sqrt{\frac{V_A}{V_{A0}}}, \quad a_- = \frac{C_{\text{refl}}}{1 + C_{\text{refl}}} a_+ \approx C_{\text{refl}} a_+.$$

We found that, for the exponential profile of the Alfvén speed, the small ratio of the amplitude of the incoming wave to that for the outgoing wave is constant. This observation, in principle, allows us to calculate the dissipation rate for the dominant wave without calculating the amplitude of the reflected wave, as long as $\Gamma_+ = \frac{1}{L_\perp} \sqrt{\frac{w_-}{\rho}} \approx C_{\text{refl}} \frac{1}{L_\perp} \sqrt{\frac{w_+}{\rho}}$. The latter

comment, although valid only for a particular case of exponentially decaying V_A , allows us to link the current model to that described in [Sokolov et al. \(2013\)](#), where we also parameterized the turbulence dissipation within the coronal holes using small dimensionless C_{refl} . The WKB approximation we used at that paper predicted no inward propagating waves originating from the open magnetic field lines ($w_- = 0$). Therefore, we assumed therein a small but finite (due to reflection) amplitude of the inward propagating wave to be parameterized as $w_- = C_{\text{refl}}^2 w_+$, so that:

$$\frac{\partial w_{\pm}}{\partial t} + \nabla \cdot [(\mathbf{u} + \mathbf{V}_A)w_{\pm}] + \frac{w_{\pm}}{2}(\nabla \cdot \mathbf{u}) = -\frac{2}{L_{\perp}} \sqrt{\frac{\max(w_{\mp}, C_{\text{refl}}^2 w_{\pm})}{\rho}} w_{\pm}. \quad (24)$$

In [Sokolov et al. \(2013\)](#) we did not discuss the reflection mechanism, so that C_{refl} was an arbitrary and uncertain free parameter. In the model developed here we calculate the reflection coefficient \mathcal{R} for realistic distribution of the magnetic field and plasma parameters, to greatly reduce the model uncertainty, however, we see that the choice of $C_{\text{refl}} = \text{const} \approx 0.01 \div 0.1$ in [Sokolov et al. \(2013\)](#) was reasonable and might be derived analytically.

In a general case of an arbitrary (not necessarily exponential) profile of the Alfvén wave speed, Eqs.(23) still can be solved at small (not necessarily constant) value of C_{refl} . Indeed, the total of two Eqs.(23) is a linear and easy-to-integrate equation, which gives: $(a_+ + a_-) \propto \sqrt{V_A}$, so that $a_+ \approx \sqrt{V_A/V_{A0}}$ as long as $a_- \ll a_+$, with constant V_{A0} , for a given thread being a characteristic value of the Alfvén wave speed at low altitude. Then, in the second of Eqs.(23) the left hand side is quadratic in small C_{refl} , as the small ($\propto C_{\text{refl}}$) derivative of a smaller amplitude, $a_- \sim C_{\text{refl}} a_+$. Therefore, the two linear in C_{refl} terms in the right hand side should cancel each other, which requirement gives: $a_- \approx -\frac{1}{2} \frac{d \log V_A}{d \xi}$. In this way, we arrive at simple and transparent estimate for the wave energy density within the coronal holes, which

linearly scales with the magnetic field: $w_+ = [\Pi/B] \sqrt{\mu_0 \rho} a_+^2 = [\Pi/B] B/V_{A0} \propto B$. From Eq.(12), we can now derive the following expressions for the heating function: $(\Gamma_+ w_+ + \Gamma_- w_-) \approx a_+^2 a_- \left(2 [\Pi/B] B \sqrt{\frac{[\Pi/B] \mu_0}{[L_\perp \sqrt{B}]^2 V_A}} \right) \approx [\Pi/B] B \frac{V_A}{V_{A0}} \left| \frac{d \log V_A}{ds} \right| = \mathcal{R} w_+ \propto B^2 / (L_{VA} \sqrt{\rho})$.

Note also that for the Alfvén speed profile gradually increasing in the outward direction, the solution for the dominant wave energy density is: $w_+ = [\Pi/B] \sqrt{\mu_0 \rho} V_{A0}/V_A \propto \rho/B$. The heating function is: $(\Gamma_+ w_+ + \Gamma_- w_-) \approx [\Pi/B] B \frac{V_{A0}}{V_A} \left| \frac{d \log V_A}{ds} \right| = \mathcal{R} w_+ \propto \sqrt{\rho}/L_{VA}$.

Now, we arrive at two important conclusions. First, within the coronal holes both the distribution of the turbulence energy and the heating function do not depend on the dissipation length, L_\perp , as long as the minor wave amplitude and the dissipation rate are fully controlled by the wave reflection. The latter, in turn, is fully controlled by the field and plasma profile. The model of a self-consistent plasma state within the coronal hole, which is controlled by the heating function dependent only on the plasma state itself, seems to be reasonable and physics-based.

However, the numerical model for the coronal hole at larger heliocentric distances, $R \approx 2 \div 10$, appears to be vulnerable to quasi-periodic formation of a narrow dip in the plasma density, with sharply peaked ion temperature amounting to 10^7 K. The dip in density corresponds to a local maximum in the Alfvén wave speed, $V_A = B/\sqrt{\mu_0 \rho}$. By merging the above given solutions for first-increasing-then-decreasing profile of the Alfvén wave speed and matching the two constant values V_{A0} to maintain the wave amplitude continuity at the maximum of V_A , one can obtain an estimate for the heating function near the density minimum: $\Gamma_+ w_+ \propto \sqrt{\rho_{\min}}/L_{VA}$. This estimate becomes large for a sharp density profile, i.e. at $L_{VA} \rightarrow 0$. The enhanced heating, which is proportional to $\propto \sqrt{\rho}$ may result in the ion temperature growth, as long as the ion specific heat effect ($\propto \rho$) and the ion-electron energy

exchange rate drop faster at $\rho \rightarrow 0$. Finally, the instability onset loop is closed by the ion thermal pressure effect, which sweeps out the locally overheated plasma and further reduces the local plasma density, ρ_{\min} , and the plasma specific heat.

Eq.(4) allows us to evaluate a threshold for the instability under consideration. The ion heating rate due to the Alfvén wave turbulence dissipation with an account of the above considerations equals $\approx f_p \mathcal{R} w_+ \approx f_p V_A w_+ / L_{V_A}$. If within the travel time, L_{V_A} / C_S , for the sound waves escaping with the sound speed, C_S , from the vicinity of the density local minimum, the ion temperature increases significantly, i.e. $(f_p V_A w_+ / L_{V_A})(L_{V_A} / C_S) > P_i / (\gamma - 1)$, the instability is possible. Therefore, the threshold condition becomes as follows: $f_p > C_S P_i / \{(\gamma - 1) V_A w_+\}$. Based on this criterion, instability is possible only in a strong turbulence, in which the turbulent energy density (flux) is comparable with that related to the thermal motion: $V_A w_+ \geq P_i C_S$.

As long as the signatures of such instability (sharp peaks in ion temperature anti-correlated with the plasma density) are not observed in the fast solar wind as originates from the coronal holes, the instability we noticed in numerous simulations should be considered as unphysical and it needs to be suppressed within the framework of numerical method. To achieve this, we limit the fraction of the turbulent energy dissipation absorbed by ions, in the regions of strong turbulence. Specifically, if $V_A w_+ \geq P_i C_S$, then instead of an equation, $f_p \approx 0.6$, we use the limited expression: $f_p = \min(0.6, C_S P_i / \{(\gamma - 1) V_A w_+\})$. There is some physical reasoning in favor of such limitation as long as if the ions are comparatively cold the number of ions which may be in gyroresonance with the Alfvén wave is small and they cannot be efficiently heated by waves. We can assume that with including the physics-based model for partitioning energy between ions and electrons (see [van der Holst et al. \(2014\)](#)) and

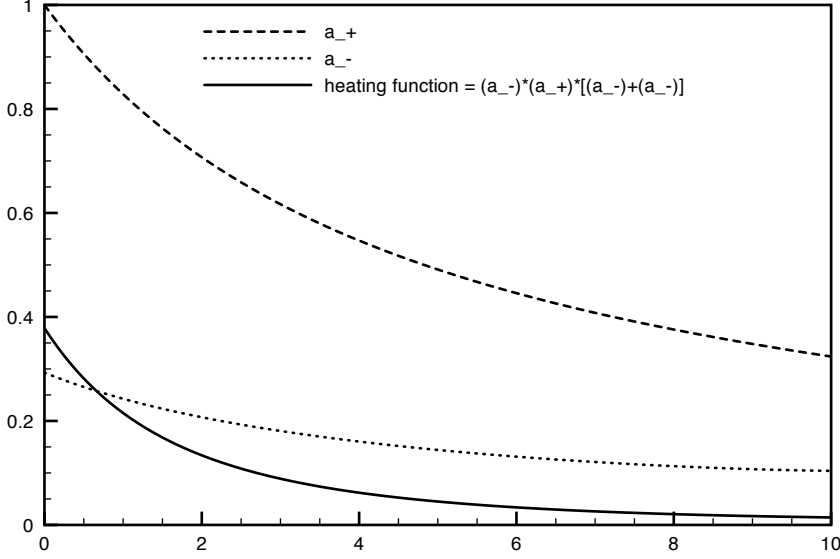


Figure 2. Dimensionless amplitudes of the Alfvén wave turbulence in a coronal hole with a strong wave reflection, $a_{\pm} = \sqrt{w_{\pm} / ([\Pi/B] \sqrt{\mu_0 \rho})}$, (dashed/dotted lines) and the dimensionless heating function, $\sum \Gamma_{\pm} w_{\pm} / \left(2 [\Pi/B] B \sqrt{\frac{[\Pi/B] \mu_0}{[L_{\perp} \sqrt{B}]^2 V_A}} \right)$ (solid line) are presented as functions of the effective magnetic field line length, $\xi(s) = \int_0^s \sqrt{\frac{[\Pi/B] \mu_0}{[L_{\perp} \sqrt{B}]^2 V_A(s')}} ds'$.

the papers cited therein), the stable model for the solar wind heating in the coronal loops may be achieved with no artificial limitation.

3.2. Coronal Holes: Strong Reflection

In the case of strong reflection, in which case the reflection coefficient in Eq.(9) is bounded with the cascade rate the governing equations for the wave dimensionless amplitude read:

$$\frac{da_+}{d\xi} = -a_-(a_+ - 2a_-) - a_-a_+, \quad \frac{da_-}{d\xi} = -a_+(a_+ - 2a_-) + a_-a_+$$

Their exact analytical solution for the coronal hole, which should tend to zero at $\xi \rightarrow \infty$ has a constant amplitude ratio, $a_-/a_+ = q < 1/2$. This ratio can be easily found by requiring that $d(a_-/a_+)/d\xi = 0$, so that $q = 1 - \sqrt{2}/2 \approx 0.29$, $a_+ = 1/\{1 + 2q(1-q)\xi\} \approx 1/(1 + 0.42\xi)$, $a_- = q/\{1 + 2q(1-q)\xi\} \approx 0.29/(1 + 0.42\xi)$. These functions and the product, $a_-a_+(a_- + a_+)$

representing the heating function, $\sum \Gamma_{\pm} w_{\pm} / \left\{ 2 \frac{B^{1/2} \rho^{1/4} \mu_0^{3/4}}{[L_{\perp} \sqrt{B}]} [\Pi/B]^{3/2} \right\}$, are plotted in Fig. 2. The heating function is maximal near the solar surface and decays with the heliocentric distance as $\propto B^{1/2} \rho^{1/4} / (1 + 0.42\xi)^3$.

3.3. *Scaling Laws for the TFLM*

The weakness of any model relying on the solar magnetogram is uncertainty of the solar magnetic field observations. We introduce the parameter of the model, $[\Pi/B] \approx 1.1 \cdot 10^6 \text{W}/(\text{m}^2 \text{T})$ with one digit after a decimal period - is this legitimate? How accurate is the observed magnitude of the solar magnetic field to be multiplied by this model parameter? Numerous observatories provide different values for the measured field. The region in the solar wind which is determined by the polar coronal holes may be large and any realistic model of the solar wind should account these holes, however, the solar magnetic field measured in these holes, by many reasons, may be unrealistically low.

To mitigate the effect of too low and, probably, underestimated magnetogram field, we apply some scaling factor $B_{\text{scale}} \geq 1$ in our simulations, so that the observed solar magnetic field multiplied by B_{scale} is used as the boundary condition of the model: $B_{\text{TFLM}}|_{R=R_{\odot}} = B_{\text{scale}} \cdot B_{\text{observed}}|_{R=R_{\odot}}$. Now, we note, that the TFLM equations keep unchanged in the course of this scaling if in accordance with increasing the magnetic field we also decrease the model parameters:

$$B \rightarrow B \cdot B_{\text{scale}}, \quad [\Pi/B] \rightarrow [\Pi/B]/B_{\text{scale}}, \quad [L_{\perp} \sqrt{B}] \rightarrow [L_{\perp} \sqrt{B}]/B_{\text{scale}}, \quad (25)$$

as long as the magnetic field in the TFLM equations is present only in combinations, $[\Pi/B]B$ and $[\Pi/B]/(B[L_{\perp} \sqrt{B}]^2)$.

4. SIMULATION RESULTS AND DISCUSSION

All simulations were performed with the Space Weather Modeling Framework (SWMF - see [Tóth et al. \(2004\)](#), [Tóth et al. \(2005\)](#), [Tóth et al. \(2007\)](#), [Tóth et al. \(2012\)](#)). The SWMF included the models (components) to simulate the Solar Corona and Inner Heliosphere, both models accounting for the contributions from the Alfvén wave turbulence as we described in [Sokolov et al. \(2013\)](#), [Oran et al. \(2013\)](#), [van der Holst et al. \(2014\)](#) (the AWSoM model). The most important distinction in the current simulations is that we apply the AWSoM model only to the GCM, while the transition region and lower corona are described using the TFLM.

In this way we benefit from saving the computational resources which otherwise should be spent to resolve the true structure of the transition region using a highly refined grid. We start from the observation that the gain in computational efficiency is achieved with no degrade in the accuracy and quality of the numerical results. In Fig. 3 we show a comparison of the numerical results obtained with the ASWoM model (see [Sokolov et al. \(2013\)](#), [Oran et al. \(2013\)](#), [van der Holst et al. \(2014\)](#)) and presented in the left panel, with the new result obtained with the TFLM (the AWSoM-R model). The grid for the AWSoM run requires much more fine grid cells to resolve the transition region. In addition, in time-dependent runs these are the finest grids which control and severely reduce the time step making is as short as a few ms. At the same time, in the AWSoM-R result (the right panel) there is no noticeable difference from that obtained with AWSoM, except that it may be obtained much faster and with the time step about one second, which is equivalent to a gain by a factor of several hundreds in the computational efficiency. The capability to do simulations well faster than the real time is the main feature of the AWSoM-R with TFLM.

We did much longer simulation to test the AWSoM-R model for the inner heliosphere.

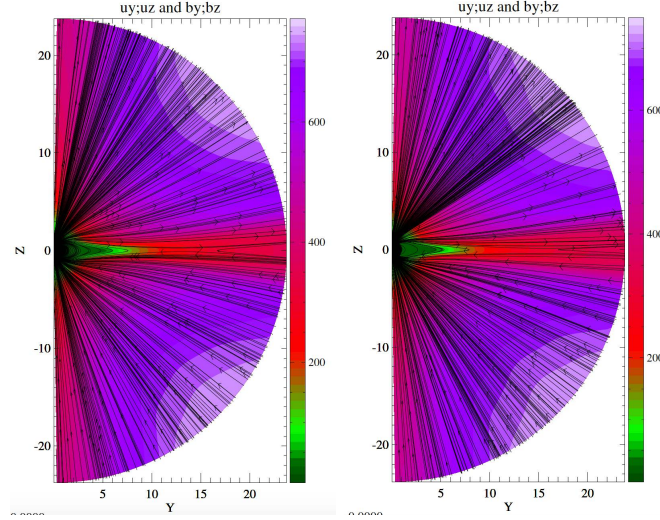


Figure 3. Steady-state solar corona with the dipole field, after 18000 iterations. Solar wind speed is shown with a color scale, black lines are the magnetic field lines. Left panel: simulation with the AWSoM model with the inner boundary at $R = R_{\odot}$. Right panel: simulation with TFLM+GCM, the interface to GCM is at $R = 1.1R_{\odot}$. The results in the GCM are practically identical with those in the AWSoM.

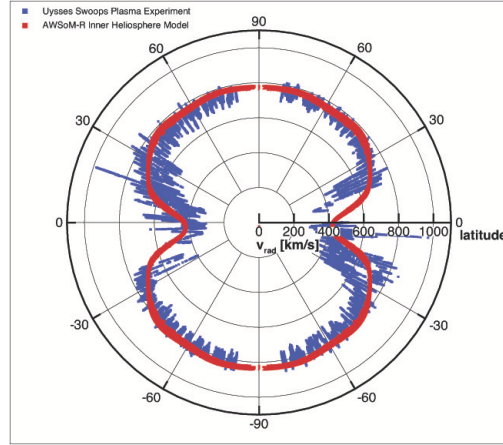


Figure 4. Polar scatterplot of the radial velocity (radius) versus the latitudinal location of the spacecraft Ulysses (angle). Blue denotes Ulysses SWOOPS data from between 1990 and 1997. Red shows the model result; the data points were sampled at the same radial distances as Ulysses passing during this period.

Specifically, using a simple dipole magnetic field as the boundary condition for the radial magnetic field component, we simulated over 47 days of physical time with the AWSoM-R

model. We sampled plasma parameters at the same distances where the Ulysses spacecraft had passed. Figure 4 shows the comparison of radial velocity distribution along different latitudes between the SWOOPS (Bame et al. 1992) plasma measurements (blue) and the simulation results (red). We selected observations of the time frame between the years 1990 and 1997 so that we cover the complete range of latitudes. The observations are during the declining phase of the solar cycle. The solar wind distribution shows the clear difference between slow and fast solar wind regions. Both these wind speeds as well as the transition latitudes are captured by the AWSoM-R model.

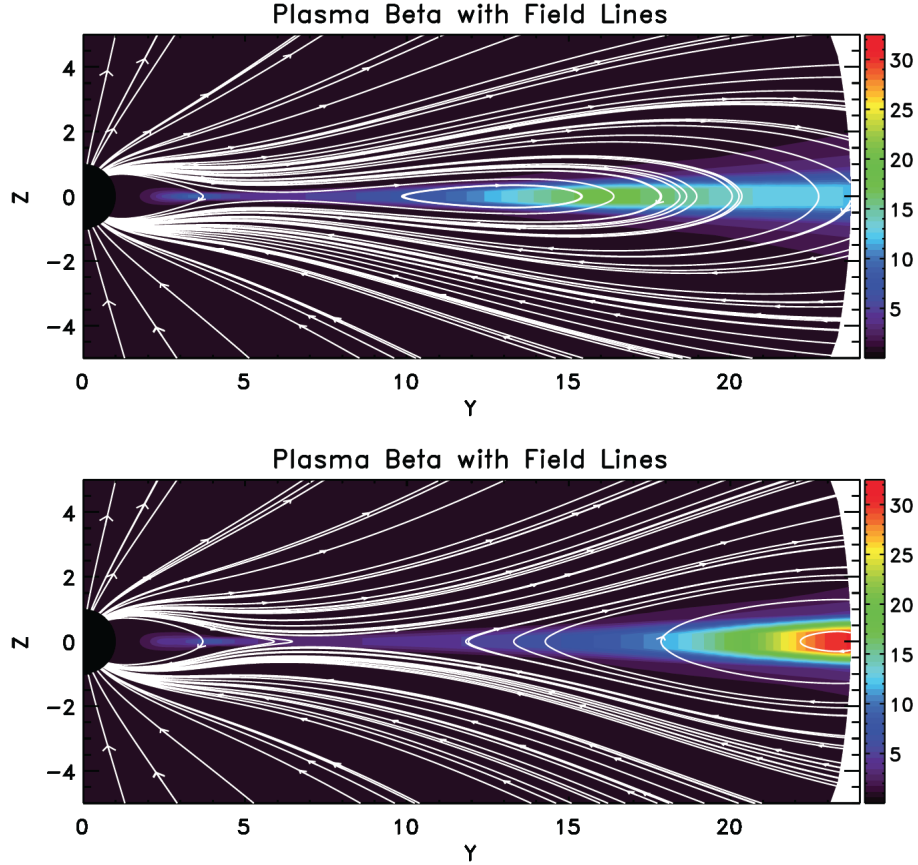


Figure 5. Variation of plasma beta and magnetic field lines along XY plane in HGR coordinates taken 6 hours 40 minutes apart. As plasma pressure increases, it stretches out the field lines (upper panel) and the reconnected field lines move anti- Sunward (lower panel)

The evolution of the solar magnetic field is comparatively slow, therefore, it is usually believed that the steady-state solution with the time independent boundary condition should be a good approximation. However, the advantage of time-dependent solution as we advocate here is in the capability to describe the processes in the solar corona which essentially involve in time even at the steady-state boundary condition for the magnetic field. To demonstrate this capability we simulated 10 days of evolution in the Solar Corona with the steady-state dipole magnetic field. Such simulation reveals a dynamic helmet streamer structure, which periodically produces plasmoids known as "streamer blobs" [Wang et al. \(2000\)](#). Our investigation shows that these blobs form as a result of pressure imbalance mainly because of increased ion temperatures at the streamer top. (see Fig.5).

To find a typical time of the blob formation, we choose a radial line in the equatorial plane rotating with the Sun (as an example we used y-axis of the HGR coordinate system) and visualize the distribution of plasma beta along this line as a function of time (x-axis) and radial coordinate(y-axis) as shown in Fig.6. The plasma beta starts increasing at the heliocentric distance of $\approx 9R_s$ implying the start of the disconnection event and the disconnected blob moves anti-Sunward. These intermittent detachment events occur with a periodicity of about 40 hours (six times within 10 days), which is in a good agreement with the observations. We, thus, show that in the self-consistent Alfvén Wave Turbulence based model the slow solar wind is intermittent even if the solar magnetic field is steady-state and perfectly symmetric.

5. CONCLUSION

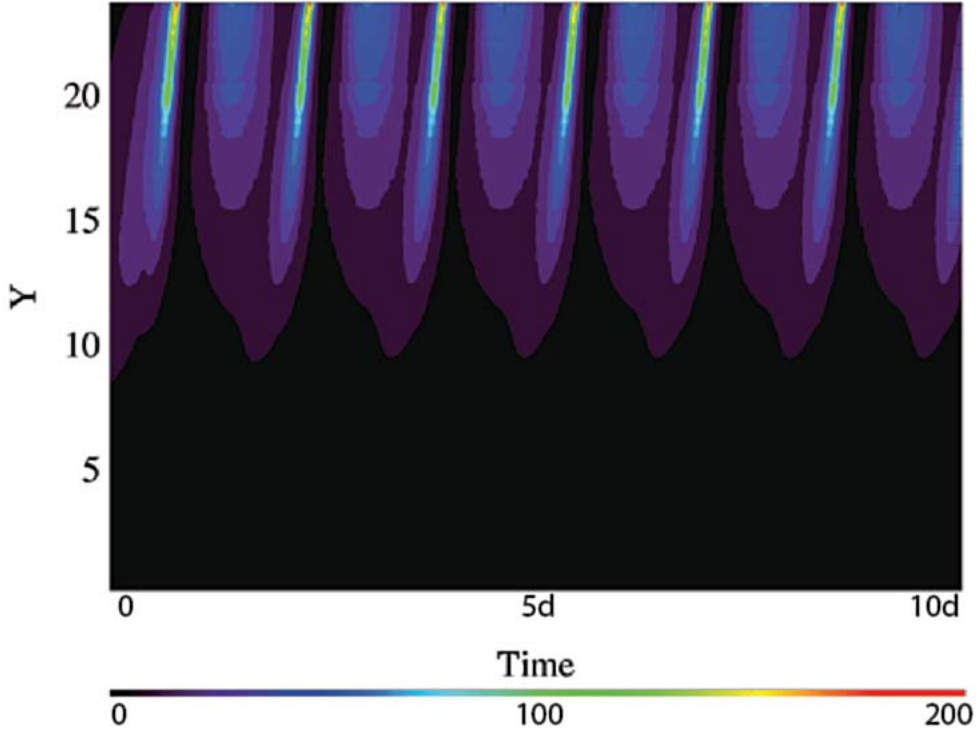


Figure 6. Plasma beta variation in the Solar Corona from the inner boundary to 25 Rs along the y-axis of the HGR coordinate system obtained from the simple dipole simulation for 10 days of physical time.

The AWSoM-R model presented here enriches the earlier developed AWSoM ([Sokolov et al. \(2013\)](#)[van der Holst et al. \(2014\)](#)) with the TFLM description for the transition region and Low Solar Corona. It allows us to simulate the Solar-Earth environments on realistic 3D grids faster than real time and with no loss in the results quality.

6. ACKNOWLEDGMENT

The collaboration between the CCMC and University of Michigan is supported by the NSF SHINE grant 1257519 (PI Aleksandre Taktakishvili). The work performed at the University of Michigan was partially supported by National Science Foundation grants AGS-1322543 and PHY-1513379, NASA grant NNX13AG25G, the European Union’s Horizon 2020 research and innovation program under grant agreement No 637302 PROGRESS. We

would also like to acknowledge high-performance computing support from: (1) Yellowstone ([ark:/85065/d7wd3xhc](https://nsls.slac.stanford.edu/ark:/85065/d7wd3xhc)) provided by NCAR's Computational and Information Systems Laboratory, sponsored by the National Science Foundation, and (2) Pleiades operated by NASA's Advanced Supercomputing Division

REFERENCES

- Abbett, W. P., The Magnetic Connection between the Convection Zone and Corona in the Quiet Sun, *Astrophys. J.*, *665*, 1469–1488, August 2007.
- Altschuler, M. D., R. H. Levine, M. Stix, J. Harvey, High Resolution Mapping of the Magnetic Field of the Solar Corona, *Solar Physics*, *51*, 345–375 (1977).
- Antiochos, S.K., DeVore, C.R., & Klimchuk, J.A., A Model for Solar Coronal Mass Ejections, *Astrophys. J.*, *510*, 485 (1999).
- Arge, C. N., and V. J. Pizzo, Improvement in the Prediction of Solar Wind Conditions Using Near-Real Time Solar Magnetic Field Updates, *J. Geophys. Res.*, *105*, 10,465–10,480, May 2000.
- Bame, S. J., McComas, D. J., Barraclough, B. L., et al. *A&AS*, *92*, 237 (1992)
- Borovikov, D., I. V. Sokolov, and G. Tóth, An Efficient Second-Order Accurate and Continuous Interpolation for Block-Adaptive Grids *J. Comp. Phys.*, *297*, 599–610 (2015)
- Chandran, B. D. G., and J. V. Hollweg, Alfvén wave reflection and turbulent heating in the solar wind from 1 solar radius to 1 au: An analytical treatment, *The Astrophysical Journal*, *707*(2), 1659, 2009.
- Chandran, B. D. G., E. Quataert, G. G. Howes, Q. Xia, and P. Pongkitiwanichakul, Constraining low-frequency alfvénic turbulence in the solar wind using density-fluctuation measurements, *The Astrophysical Journal*, *707*(2), 1668, 2009.
- Cohen, O., I. V. Sokolov, I. I. Roussev, C. N. Arge, W. B. Manchester, T. I. Gombosi, R. A. Frazin, H. Park, M. D. Butala, F. Kamalabadi, and M. Velli, A Semiempirical Magnetohydrodynamical Model of the Solar Wind, *Astrophys. J. Lett.*, *654*, L163–L166, January 2007.
- Cohen, O., I. V. Sokolov, I. I. Roussev, and T. I. Gombosi, Validation of a Synoptic Solar Wind Model, *J. Geophys. Res. (Space Physics)*, *113*(A12), A03104, March 2008.
- Cranmer, S. R., An Efficient Approximation of the Coronal Heating Rate for use in Global Sun-Heliosphere Simulations, *Astrophys. J.*, *710*, 676–688, February 2010.
- De Pontieu, B., S. W. McIntosh, M. Carlsson, V. H. Hansteen, T. D. Tarbell, C. J. Schrijver, A. M. Title, R. A. Shine, S. Tsuneta, Y. Katsukawa, K. Ichimoto, Y. Suematsu, T. Shimizu, and S. Nagata, Chromospheric Alfvénic Waves Strong Enough to Power the Solar Wind, *Science*, *318*, 1574–, December 2007.
- Dmitruk, P., W. H. Matthaeus, L. J. Milano, S. Oughton, G. P. Zank, and D. J. Mullan, Coronal Heating Distribution Due to Low-Frequency, Wave-driven Turbulence, *Astrophys J.*, *575*, 571–577, August 2002.
- Downs, C., Roussev, I.I., van der Holst, B., Lugaz, N., Sokolov, I.V., Gombosi, T.I., Toward a Realistic Thermodynamic Magnetohydrodynamic Model of the Global Solar Corona, *Astrophys. J.*, *712*, 1219 (2010).
- Fan Y. & Gibson, S.E., Numerical Simulations of Three-dimensional Coronal Magnetic Fields Resulting from the Emergence of Twisted Magnetic Flux Tubes, *Astrophys. J.*, *609*, 1123 (2004).
- Hollweg, J. V., Transition Region, Corona and Solar Wind in Coronal Holes, *J. Geophys. Res.*, *91*, 1411–1425, April 1986.
- Hu, Y. Q., R. Esser, and S. R. Habbal, A four-fluid turbulence-driven solar wind model for preferential acceleration and heating of heavy ions, *J. Geophys. Res.*, *105*, 5093–5112, March 2000.
- Gombosi, T. I., G. Tóth, D. L. DeZeeuw, K. C. Hansen, K. Kabin and K. G. Powell, *J. Comput. Phys.*, *177*, 176, 2002
- Gosling, J.T., The solar flare myth, *J. Geophys. Res.*, *98*, 18937 (1993).
- Groth, C. P. T., D. L. DeZeeuw, T. I. Gombosi, and K. G. Powell, Global Three-Dimensional MHD Simulation of a Space Weather Event: CME Formation, Interplanetary Propagation, and Interaction with the Magnetosphere, *J. Geophys. Res.*, *105*, 25,053–25,078, November 2000.
- Jacobs, C., I. I. Roussev, N. Lugaz, and S. Poedts, The Internal Structure of Coronal Mass Ejections: Are all Regular Magnetic Clouds Flux Ropes?, *Astrophys. J. Lett.*, *695*, L171–L175, April 2009.
- Jin, M., Manchester, W.B., van der Holst, B., Gruesbeck, J.R., Frazin, R.A., Landi, E., Vasquez, A.M., Lamy, P.L., Llebaria, A., Fedorov, A., Toth, G., & Gombosi, T.I., A Global Two-temperature Corona and Inner Heliosphere Model: A Comprehensive Validation Study, *Astrophys. J.*, *745*, 6 (2012).
- Jin, M., W. B. Manchester, B. van der Holst, R. Oran, I. Sokolov, G. Toth, Y. Liu, X. D. Sun, and T. I. Gombosi, Numerical simulations of coronal mass ejection on 2011 march 7: One-temperature and two-temperature model comparison, *The Astrophysical Journal*, *773*(1), 50, 2013.
- Li, X., and S. R. Habbal, Coronal Loops Heated by Turbulence-driven Alfvén Waves, *Astrophys J.*, *598*, L125–L128, December 2003.
- Lionello, R., J. A. Linker, and Z. Mikić, Including the Transition Region in Models of the Large-Scale Solar Corona, *Astrophys. J.*, *546*, 542–551, January 2001.

- Lionello, R., J. A. Linker, and Z. Mikić, Multispectral Emission of the Sun During the First Whole Sun Month: Magnetohydrodynamic Simulations, *Astrophys. J.*, **690**, 902–912, January 2009.
- Manchester, W. B., T. I. Gombosi, I. Roussev, D. L. De Zeeuw, I. V. Sokolov, K. G. Powell, G. Tóth, and M. Opher, Three-Dimensional MHD Simulation of a Flux Rope Driven CME, *J. Geophys. Res.*, **109(A18)**, 1,102–1,119, January 2004a.
- Manchester, W. B., T. I. Gombosi, I. Roussev, A. Ridley, D. L. De Zeeuw, I. V. Sokolov, K. G. Powell, and G. Tóth, Modeling a Space Weather Event from the Sun to the Earth: CME Generation and Interplanetary Propagation, *J. Geophys. Res.*, **109(A18)**, 2,107–2,122, February 2004b.
- Manchester, W. B., T. I. Gombosi, D. L. De Zeeuw, I. V. Sokolov, I. I. Roussev, K. G. Powell, J. Kóta, G. Tóth, and T. H. Zurbuchen, Coronal Mass Ejection Shock and Sheath Structures Relevant to Particle Acceleration, *Astroph. J.*, **622**, 1225–1239, April 2005.
- Manchester IV, W.B., van der Holst, B., Tóth, G., & Gombosi, T.I., ‘The Coupled Evolution of Electrons and Ions in Coronal Mass Ejection-driven shocks’, *Astrophys. J.*, **756**, 81 (2012).
- Matthaeus, W. H., G. P. Zank, S. Oughton, D. J. Mullan, and P. Dmitruk, Coronal heating by magnetohydrodynamic turbulence driven by reflected low-frequency waves, *The Astrophysical Journal Letters*, **523**(1), L93, 1999.
- McIntosh, S. W., B. de Pontieu, M. Carlsson, V. Hansteen, P. Boerner, and M. Goossens, Alfvénic waves with sufficient energy to power the quiet solar corona and fast solar wind, *Nature*, **475**, 477–480, July 2011.
- Lugaz, N., W. B. Manchester, IV, I. I. Roussev, G. Tóth, and T. I. Gombosi, Numerical Investigation of the Homologous Coronal Mass Ejection Events from Active Region 9236, *Astroph. J.*, **659**, 788–800, April 2007.
- Ogino, T., and Walker R. J., *Geophys. Res. Lett.*, **11**, 1018, 1984.
- Oran, R., B. van der Holst, E. Landi, M. Jin, I. V. Sokolov, and T. I. Gombosi, A Global Wave-Driven MHD Solar Model with a Unified Treatment of Open and Closed Magnetic Field Topologies, *Astroph. J.*, **778**, 176, July 2013.
- Osman, K. T., W. H. Matthaeus, A. Greco, and S. Servidio, Evidence for Inhomogeneous Heating in the Solar Wind, *Astrophys. J. Lett.*, **727**(1), January 2011.
- Pevtsov, A. A., G. H. Fisher, L. W. Acton, D. W. Longcope, C. M. Johns-Krull, C. C. Kankelborg, and T. R. Metcalf, The Relationship Between X-Ray Radiance and Magnetic Flux, *Astrophys. J.*, **598**, 1387–1391, December 2003.
- Powell, K. G., P. L. Roe, T. J. Linde, T. I. Gombosi, and D. L. De Zeeuw, A Solution-Adaptive Upwind Scheme for Ideal Magnetohydrodynamics, *J. Comp. Phys.*, **154**, 284–309, September 1999.
- Riley, P., J. A. Linker, Z. Mikić, R. Lionello, S. A. Ledvina, and J. G. Luhmann, A Comparison between Global Solar Magnetohydrodynamic and Potential Field Source Surface Model Results, *Astrophys. J.*, **653**, 1510–1516, December 2006.
- Roussev, I. I., T. I. Gombosi, I. V. Sokolov, M. Velli, W. Manchester, D. L. DeZeeuw, P. Liewer, G. Tóth, and J. Luhmann, A Three-Dimensional Model of the Solar Wind Incorporating Solar Magnetogram Observations, *Astrophys. J. Lett.*, **595**, L57–L61, September 2003.
- Roussev, I. I., T. G. Forbes, T. I. Gombosi, I. V. Sokolov, D. L. DeZeeuw, and J. Birn, A Three-Dimensional Flux Rope Model for Coronal Mass Ejections Based on a Loss of Equilibrium, *Astrophys. J. Lett.*, **588**, L45–L48, May 2003a.
- Roussev, I. I., I. V. Sokolov, T. G. Forbes, T. I. Gombosi, M. A. Lee, and J. I. Sakai, A Numerical Model of a Coronal Mass Ejection: Shock Development with Implications for the Acceleration of GeV Protons, *Astrophys. J. Lett.*, **605**, L73–L76, April 2004.
- Roussev, I. I., N. Lugaz, and I. V. Sokolov, New Physical Insight on the Changes in Magnetic Topology during Coronal Mass Ejections: Case Studies for the 2002 April 21 and August 24 Events, *Astrophys. J. Lett.*, **668**, L87–L90, October 2007.
- Sokolov, I. V., I. I. Roussev, T. I. Gombosi, M. A. Lee, J. Kóta, T. G. Forbes, W. B. Manchester, and J. I. Sakai, A New Field-Line-Advection Model for Solar Particle Acceleration, *Astrophys. J. Lett.*, **616**, L171–L174, December 2004.
- Sokolov, I. V., I. I. Roussev, L. A. Fisk, M. A. Lee, T. I. Gombosi, and J. I. Sakai, Diffusive Shock Acceleration Theory Revisited, *Astrophys. J. Lett.*, **642**, L81–L84, May 2006.
- Sokolov, I. V., B. van der Holst, R. Oran, C. Downs, I. I. Roussev, M. Jin, W. B. Manchester, IV, R. M. Evans, and T. I. Gombosi, Magnetohydrodynamic Waves and Coronal Heating: Unifying Empirical and MHD Turbulence Models, *Astrophys. J.*, **764**, 23, February 2013.
- Suzuki, T. K., and S.-i. Inutsuka, Making the Corona and the Fast Solar Wind: A Self-consistent Simulation for the Low-Frequency Alfvén Waves from the Photosphere to 0.3 AU, *Astrophys. J. Lett.*, **632**, L49–L52, October 2005.
- Suzuki, T. K., Forecasting Solar Wind Speeds, *Astrophys. J. Lett.*, **640**, L75–L78, March 2006.
- Tanaka, T., *J. Comput. Phys.*, **111**, 381, 1994.

- Titov, V. S., Z. Mikic, J. A. Linker, and R. Lionello, 1997 May 12 Coronal Mass Ejection Event. I. A Simplified Model of the Preeruptive Magnetic Structure, *Astrophys. J.*, **675**, 1614–1628, March 2008.
- Torok, T. & Kliem, B., Confined and Ejective Eruptions of Kink-unstable Flux Ropes, *Astrophys. J.*, **630**, L97 (2005).
- Tóth, G., O. Volberg, A. J. Ridley, T. I. Gombosi, D. L. DeZeeuw, K. C. Hansen, D. Chesney, Q. F. Stout, K. G. Powell, K. Kane, and R. Oehmke, A Physics-Based Software Framework for Sun-Earth Connection Modeling, In Lui, A. T. Y., Y. Kamide, and G. Consolini, editors, *Proc. of the Conf. on the Sun-Earth Connection: Multi-scale Coupling of Sun-Earth Processes*. Elsevier Publ. Co.: Amsterdam, The Netherlands, 2004.
- Tóth, G., I. V. Sokolov, T. I. Gombosi, D. R. Chesney, C. R. Clauer, D. L. De Zeeuw, K. C. Hansen, K. J. Kane, W. B. Manchester, R. C. Oehmke, K. G. Powell, A. J. Ridley, I. I. Roussev, Q. F. Stout, O. Volberg, R. A. Wolf, S. Sazykin, A. Chan, B. Yu, and J. Kóta, Space Weather Modeling Framework: A New Tool for the Space Science Community, *J. Geophys. Res.*, **110**, 12,226–12,237, December 2005.
- Toth, G., De Zeeuw, D.L., Gombosi, T.I., Manchester, W.B., Ridley, A.J., Sokolov, I.V., & Roussev, I.I., Sun-to-thermosphere simulation of the 28-30 October 2003 storm with the Space Weather Modeling Framework, *Space Weather*, **5**, 6003 (2007).
- Tóth, G., van der Holst, B., Sokolov, I.V., De Zeeuw, D.L., Gombosi, T.I., Fang, F., Manchester, W.B., Meng, X., Najib, D., Powell, K.G., Stout, Q.F., Gloer, A., Ma, Y.-J., & Opher, M., Adaptive numerical algorithms in space weather modeling, *J. Comp. Phys.*, **231**, 870 (2012).
- Tu, C.-Y., and E. Marsch, MHD structures, waves and turbulence in the solar wind: Observations and theories, *Space Sci. Rev.*, **73**, 1–210, July 1995.
- Tu, C.-Y., and E. Marsch, Two-Fluid Model for Heating of the Solar Corona and Acceleration of the Solar Wind by High-Frequency Alfvén Waves, *Solar Phys.*, **171**, 363–391, April 1997.
- Usmanov, A. V., M. L. Goldstein, B. P. Besser, and J. M. Fritzer, A Global MHD Solar Wind Model with WKB Alfvén Waves: Comparison with Ulysses Data, *J. Geophys. Res.*, **105**, 12,675–12,696, June 2000.
- van der Holst, B., W. B. Manchester, IV, R. A. Frazin, A. M. Vásquez, G. Tóth, and T. I. Gombosi, A Data-driven, Two-temperature Solar Wind Model with Alfvén Waves, *Astrophys. J.*, **725**, 1373–1383, December 2010.
- van der Holst, B., Igor V. Sokolov, Xing Meng, Meng Jin, W. B. Manchester, IV, G. Tóth, and T. I. Gombosi, Alfvén Wave Solar Model (AWSOM): Coronal Heating, *Astrophys. J.*, **782**, 81, February 2014.
- Velli, M., On the propagation of ideal, linear Alfvén waves in radially stratified stellar atmospheres and winds, *Astronomy & Astrophysics*, **270**, 304–314, March 1993.
- Verdini, A., M. Velli, W. H. Matthaeus, S. Oughton, and P. Dmitruk, A Turbulence-Driven Model for Heating and Acceleration of the Fast Wind in Coronal Holes, *Astrophys. J. Lett.*, **708**, L116–L120, January 2010.
- Wang, Y. M., Sheeley, N. R., Socker, D. G., Howard, R. A., Rich, N. B., The dynamical nature of coronal streamers, *Journal of Geophysical Research* **105**, 133–142, November 2000